# Journal of Materials Chemistry A



# COMMUNICATION

View Article Online



Cite this: J. Mater. Chem. A, 2018, 6,

Received 29th December 2017 Accepted 19th February 2018

DOI: 10.1039/c7ta11347a

rsc.li/materials-a

# Effect of glycine functionalization of 2D titanium carbide (MXene) on charge storage†

Chi Chen, ab Muhammad Boota, a Patrick Urbankowski, Babak Anasori, a Ling Miao, b Jianjun Jiang \*b and Yury Gogotsi \*b \*a

Restacking of two-dimensional (2D) flakes reduces the accessibility of electrolyte ions and is a problem in energy storage and other applications. Organic molecules can be used to prevent restacking and keep the interlayer space open. Here, we report on a combined theoretical and experimental investigation of the interaction between 2D titanium carbide (MXene), Ti<sub>3</sub>C<sub>2</sub>T<sub>x</sub>, and glycine. From first principle calculations, we presented the functionalization of glycine on the Ti<sub>3</sub>C<sub>2</sub>O<sub>2</sub> surface, evidenced by the shared electrons between Ti and N atoms. To experimentally validate our predictions, we synthesized flexible freestanding films of Ti<sub>3</sub>C<sub>2</sub>T<sub>x</sub>/glycine hybrids. X-ray diffraction and X-ray photoelectron spectroscopy confirmed the increased interlayer spacing and possible Ti-N bonding, respectively, which agree with our theoretical predictions. The Ti<sub>3</sub>C<sub>2</sub>T<sub>x</sub>/glycine hybrid films exhibited an improved rate and cycling performances compared to pristine Ti<sub>3</sub>C<sub>2</sub>T<sub>x</sub>, possibly due to better charge percolation within expanded  $Ti_3C_2T_x$ .

# Introduction

Understanding the interactions between organic and inorganic constituents of hybrid materials is of fundamental importance for modifying their surfaces/interfaces to further expand their applications. These interactions can be divided into two types: (1) physical and (2) chemical. Introduction of organic molecules into inorganic matrices typically uses weak physical interactions, such as van der Waals forces, 1,2 hydrogen bonding3 and  $\pi$ - $\pi$  interactions.<sup>4</sup> On the other hand, chemical interactions induce strong coupling between organic and inorganic components of hybrid materials, usually resulting in chemical bonding.5,6 Interactions via chemical bonding strongly affect the electronic<sup>7,8</sup> and optoelectronic<sup>9</sup> properties, which, in turn, also could lead to improved charge storage performance of the hybrid materials in energy storage systems.10

2D inorganic materials have garnered immense interest due to their unique properties. More than 20 2D transition metal carbides and/or nitrides named MXenes with a general formula of  $M_{n+1}X_nT_x$  have been obtained by selectively etching the A-group element layers from their ternary carbide or nitride precursors, such as MAX phases.11-15 In MXenes, M is an early transition metal, and X is carbon and/or nitrogen, n = 1, 2, or 3, and Tx refers to surface terminations such as OH, O and F. 11,16,17 MXenes have been combined with carbon nanomaterials (e.g., graphene, 18,19 carbon nanotubes, 20,21 etc.), metal oxides, 22,23 polymers<sup>24-28</sup> mostly via intermolecular forces or electrostatic interactions. Also, some organic molecules have been investigated, with a focus on their effects on the intercalation and delamination of MXenes.<sup>29-31</sup> While some progress has been made to hybridize MXene with other materials, the fundamental understanding of MXene surface interactions with organic molecules is still to be achieved.

Amino acids, vital in living organisms as building blocks of proteins and enzymes, can be used to functionalize nanomaterials and efforts have been made to study their interaction mechanism with a variety of 2D materials, such as graphene, h-BN and h-SiC.32-34 Furthermore, these interactions have been applied for reduction of graphene oxide,35 intercalation and functionalization of MoS2.36 Unlike most of other 2D materials, MXenes offer a unique combination of properties such as hydrophilicity, metallic conductivity and structural diversity. Nevertheless, to date, there is no report available on the interaction of amino acids with MXenes, even though biomedical applications of MXenes are emerging.37-39 Their interactions with MXene surfaces may have an impact on properties of MXenes, including charge storage performance biocompatibility.

In this study, we used first principle calculations to discuss the interaction mechanism between the most studied MXene, Ti<sub>3</sub>C<sub>2</sub>T<sub>x</sub>, and the simplest amino acid - glycine. Experimentally,

<sup>&</sup>lt;sup>a</sup>A.J. Drexel Nanomaterials Institute, Materials Science and Engineering Department, Drexel University, 3141 Chestnut Street, Philadelphia, PA 19104, USA. E-mail: gogotsi@drexel.edu

<sup>&</sup>lt;sup>b</sup>School of Optical and Electronic Information, Huazhong University of Science and Technology, Wuhan, Hubei 430074, People's Republic of China. E-mail: jiangjj@

<sup>†</sup> Electronic supplementary information (ESI) available: Experimental details and Fig. S1-S4. See DOI: 10.1039/c7ta11347a

we synthesized MXene/amino acid hybrids and characterized them by various spectroscopic techniques. Finally, we discuss the impact of the interaction of glycine with  ${\rm Ti_3C_2T_x}$  on its pseudocapacitance.

# Experimental and computational details

 $Ti_3C_2T_x$  was synthesized following previous work.<sup>25</sup> Briefly, LiF (2 g) was stirred in HCl (9 M, 20 ml) for 5 minutes followed by slow addition of  $Ti_3AlC_2$  (2 g) powder. The solution was stirred for 24 h at 35 °C. After that, multilayer  $Ti_3C_2T_x$  was obtained by washing with deionized (DI) water *via* centrifugation and decantation several times until the pH of the supernatant fluid reached  $\sim$ 6. A delaminated  $Ti_3C_2T_x$  solution (d- $Ti_3C_2T_x$ ) was made by re-dispersing 1 g of the as-prepared dry multilayer  $Ti_3C_2T_x$  into DI water and sonicating for 1.5 h under Ar flow. After centrifugation at 3500 rpm for 1 h, the supernatant was collected as the d- $Ti_3C_2T_x$  solution.

To prepare d-Ti $_3C_2T_x$ /amino acid hybrids, we selected two common amino acids named glycine ( $C_2H_5NO_2$ ) and leucine ( $C_6H_{13}NO_2$ ). The d-Ti $_3C_2T_x$ /amino acid hybrids were synthesized as follows: amino acid powders (5 mg glycine, 50 mg glycine, or 5 mg leucine) were dissolved into 20 ml of DI water by stirring at room temperature. Then, 10 ml of d-Ti $_3C_2T_x$  solution (1.0 mg ml $^{-1}$ ) was added dropwise and stirred for 24 h at room temperature. After that, the solutions were vacuum filtered and washed with DI water to get the freestanding flexible films. All samples were vacuum dried at 200 °C for 12 h, labeled as d-Ti $_3C_2T_x$ /glycine, d-Ti $_3C_2T_x$ /glycine-H (higher initial mass of glycine, 50 mg) and d-Ti $_3C_2T_x$ /leucine.

First-principle calculations were performed using VASP code, <sup>40</sup> based on density-functional theory (DFT). <sup>41,42</sup> The exchange–correlation energy was calculated using general gradient approximation (GGA) with the Perdew–Burke–Ernzerhof (PBE) exchange–correlation functional. <sup>43</sup> The effect of van der Waals interactions was estimated, implemented in the optimized exchange van der Waals functional B86b of the Becke (optB86b vdW) functional. <sup>44,45</sup> The convergence condition for the energy was 10<sup>-4</sup> eV, and the structures were relaxed until the force on each atom was less than 0.03 eV Å<sup>-1</sup>. Spin polarization was considered in all calculations.

It has been demonstrated previously that the major surface groups (up to  ${\sim}85\%$ ) are O groups for LiF–HCl synthesized  $\rm Ti_3C_2T_x$ .  $^{46}$  Therefore, the DFT discussions focus on the  $\rm Ti_3C_2O_2$  structure. The 4  $\times$  4 supercells of single-layer  $\rm Ti_3C_2O_2$  was chosen as substrate for glycine, and double-layer structure was adopted to discuss the influence of glycine on the interlayer spacing of  $\rm Ti_3C_2O_2$  layers. The c axes were set as 30 and 40 Å for single- and double-layer models to ensure enough vacuum to avoid interactions between two periods. The plane wave cutoff energy was 580 eV and the k-point meshes of 3  $\times$  3  $\times$  1 and 5  $\times$  5  $\times$  1 in the Monkhorst–Pack sampling scheme  $^{47}$  were used for geometry optimization and energy calculation, respectively. The structures and charge density visualization were generated using VESTA.  $^{48}$ 

# Results and discussion

## Interaction between glycine and titanium carbide

The amino acids contain amine  $(-NH_2)$  and carboxyl (-COOH) functional groups, along with a side chain specific for each amino acid. Glycine is the simplest amino acid with a hydrogen atom at its side chain (Fig. 1a), which could be considered as a model system to discuss the interactions between amino acids and MXenes at minimal computational cost. Using first-principle calculations, we first investigated the adsorption behaviors of glycine on  $Ti_3C_2O_2$  surface (Fig. 1). The binding energy of glycine on the surface of  $Ti_3C_2O_2$  is defined as:

$$E_{\rm b} = E_{\rm MXene+glycine} - (E_{\rm MXene} + E_{\rm glycine}),$$

where  $E_{\rm MXene+glycine}$  is the total energy of glycine adsorbed on the surface of Ti<sub>3</sub>C<sub>2</sub>O<sub>2</sub>,  $E_{\rm MXene}$  is the total energy of Ti<sub>3</sub>C<sub>2</sub>O<sub>2</sub> and  $E_{\rm glycine}$  is the total energy of glycine. The adsorption configurations and corresponding binding energies are shown in Fig. 1a, which are within the range between -0.75 to -0.32 eV. The configuration with the N atom facing a Ti atom (Fig. 1a top left) is the most stable one for glycine on the Ti<sub>3</sub>C<sub>2</sub>O<sub>2</sub> surface with the highest binding energy of -0.75 eV.

The strong interactions between glycine and  $Ti_3C_2O_2$  can be explained by the large charge transfer between glycine and  $Ti_3C_2O_2$  (Fig. 1b). According to Bader analysis, <sup>49</sup> 0.31 electrons transfer from glycine to  $Ti_3C_2O_2$ , resulting in the decreased valence of N atom from -1.08(7) to -1.09(2) and increased valence for the corresponding Ti atom from +1.69(1) to +1.72(3). Importantly, the shared electrons accumulated between N and Ti atoms could be observed from the electronic charge density difference contour (Fig. 1c). Therefore, it is reasonable to conclude that the Ti–N bond might form by shared electrons

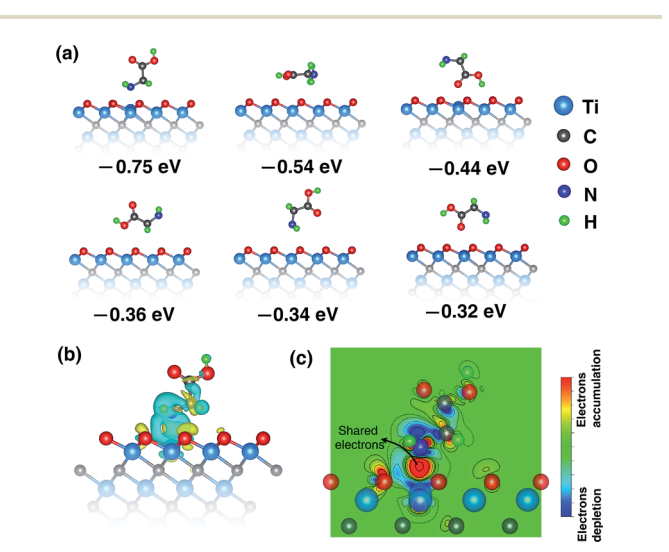


Fig. 1 (a) Different adsorption configurations and corresponding binding energies of glycine on the surface of  $Ti_3C_2O_2$  (top views of the adsorption configurations are given in Fig. S1†). (b) Difference of charge density for the most stable adsorption configuration, top left in (a). The blue and yellow regions indicate depletion and accumulation of electrons, respectively, (c) the electronic charge density difference contour on adsorption plane.

with a bond length of 2.35(8) Å. These results show that the chemical interaction occurs between glycine and  $Ti_3C_2O_2$ .

#### Characterizations of the hybrid films

Communication

To confirm our predictions, we prepared the freestanding and flexible films (Fig. 2a) by mixing d-Ti<sub>3</sub>C<sub>2</sub>T<sub>x</sub> and glycine solutions with the ratios that were mentioned in the Experimental section. The obtained hybrid maintained the layered structure of MXene, as shown in cross-sectional SEM image (Fig. 2b). The presence and interaction of glycine with d-Ti<sub>3</sub>C<sub>2</sub>T<sub>x</sub> layers was confirmed by spectroscopic techniques. Fig. 2c shows the Raman spectra of pristine d-Ti<sub>3</sub>C<sub>2</sub>T<sub>x</sub>, glycine, and the as-prepared d-Ti<sub>3</sub>C<sub>2</sub>T<sub>x</sub>/glycine hybrid films. The spectrum of the hybrid film showed a combined character of glycine and pristine d-Ti<sub>3</sub>C<sub>2</sub>T<sub>x</sub>, indicating the presence of glycine between/on MXene layers. The 1442, 1367 and 1291 cm<sup>-1</sup> bands are attributed to the C-H stretching or twisting from -CH<sub>2</sub>- group, and the bands at 1146 and 1536 cm<sup>-1</sup> are ascribed to the N-H vibrations of amino group. 50-52 Importantly, the band at 893 cm<sup>-1</sup>, that is for C-C-N stretching<sup>53,54</sup> in glycine, disappeared from the spectrum of the d-Ti<sub>3</sub>C<sub>2</sub>T<sub>x</sub>/glycine hybrid, showing the suppression of C-C-N vibrations. Meanwhile, it can be seen that the d-Ti<sub>3</sub>C<sub>2</sub>T<sub>r</sub> bands<sup>11</sup> and sharp glycine bands appear stretched, confirming likely interaction within the hybrid structure.

The vibrational bands in the FTIR spectrum (Fig. 2d) of the  $d-Ti_3C_2T_x/g$ lycine hybrid film at about 1640 and 1444 cm<sup>-1</sup> are

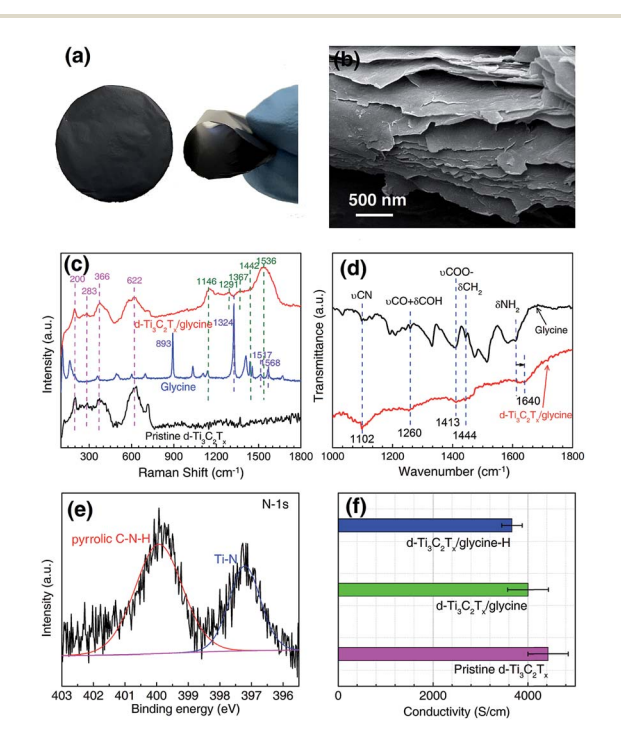


Fig. 2 (a) The freestanding and flexible film of d- $Ti_3C_2T_x$ /glycine hybrid, (b) cross-sectional SEM image of the d- $Ti_3C_2T_x$ /glycine film, (c) comparison of Raman spectra for pristine d- $Ti_3C_2T_x$ , glycine and d- $Ti_3C_2T_x$ /glycine, (d) FTIR spectrum for glycine and d- $Ti_3C_2T_x$ /glycine. (e) XPS pattern of d- $Ti_3C_2T_x$ /glycine, (f) electrical conductivity of pristine d- $Ti_3C_2T_x$ , d- $Ti_3C_2T_x$ /glycine and d- $Ti_3C_2T_x$ /glycine-H hybrids.

attributed to the bending of  $-\mathrm{NH_2}$  and  $-\mathrm{CH_2}-$  groups, respectively. Notably, the amine vibration band at 1640 cm<sup>-1</sup> is strongly blue-shifted, which corroborates our theoretical results, suggesting that amine groups strongly interact with the  $\mathrm{Ti_3C_2T_x}$  surface. The band seen at around 1413 cm<sup>-1</sup> is due to stretching of the  $-\mathrm{COO}$  group. The stretching of  $-\mathrm{CO}$  and bending of  $-\mathrm{COH}$  are observed at around 1260 cm<sup>-1</sup>. The band at 1102 cm<sup>-1</sup> could be ascribed to the stretching of  $-\mathrm{CN}$  group. 55-58 Spectroscopic results presented here confirm that glycine has been hybridized within the d- $\mathrm{Ti_3C_2T_x}$  layers.

The interaction/bonding between glycine and d-Ti<sub>3</sub>C<sub>2</sub>T<sub>x</sub> layers was further investigated by XPS, as shown in Fig. 2e for the N-1s spectra. Despite the peak at 399.9 eV from pyrrolic C–N–H in glycine, the other peak at 397.2 eV suggests the formation of Ti–N bonds, <sup>59</sup> which corroborates our theoretical prediction of surface functionalization of d-Ti<sub>3</sub>C<sub>2</sub>T<sub>x</sub> by glycine. These peaks were of a much lower intensity than other scanned regions, due to the low glycine content in the hybrid, which was  $\sim\!4.65\%$  by thermogravimetric analysis (Fig. S2†). Meanwhile, this peak at 397.2 eV may possibly correspond to the adsorption of N-containing molecules on a Ti surface, a phenomenon that occurs for samples in XPS by electron stimulated formation. <sup>60,61</sup>

We further measured the electrical conductivity by the four-point probe method (Fig. 2f), and obtained values of  $4425 \pm 425$  and  $4002 \pm 431~S~cm^{-1}$  for pristine d-Ti $_3$ C $_2$ T $_x$  and d-Ti $_3$ C $_2$ T $_x$ /glycine hybrid films, respectively. When we increased the initial amount of glycine in the hybrid (d-Ti $_3$ C $_2$ T $_x$ /glycine-H), the conductivity of the hybrid decreased to  $3663 \pm 215~S~cm^{-1}$ , most likely due to increased amount of poorly conducting glycine between the MXene sheets.

### Charge storage performance

We then turn our attention to the influence of the glycine functionalization on MXene interlayer spacing from both theoretical and experimental perspectives. According to our first principle calculations, the interlayer spacing of pristine of  $Ti_3C_2O_2$  is 10.16 Å (Fig. S3†), which is in agreement with the earlier reports. 62,63 Nevertheless, MXenes are hydrophilic, 64 and there will be intercalation of water during synthesis of the hybrids at ambient conditions due to humidity of air. Also, it is difficult to completely remove the water molecules from MXene layers without high-temperature treatment. Therefore, it is reasonable to calculate the interlayer spacing with intercalated water, and three possible configurations are considered as shown in Fig. S4.† The most stable orientation of water is shown in the bottom right illustration of Fig. 3a, with an interlayer spacing of 12.87 Å. Furthermore, the chemical bonding of glycine on Ti<sub>3</sub>C<sub>2</sub>O<sub>2</sub> will lead to expansion of the interlayer spacing to 14.06 Å (Fig. 3a, right top), with increment of 1.19 Å compared with the water-intercalated model. On the other hand, XRD patterns of the pristine  $d-Ti_3C_2T_x$ ,  $d-Ti_3C_2T_x$ /glycine films are shown in Fig. 3a (left), with (002) peaks at  $\sim$ 7.38° and 6.72°, respectively. The interlayer spacing of d-Ti<sub>3</sub>C<sub>2</sub>T<sub>x</sub>/glycine hybrid is  $\sim$ 1.22 Å larger than pristine d-Ti<sub>3</sub>C<sub>2</sub>T<sub>x</sub>, which agrees with our theoretical prediction.

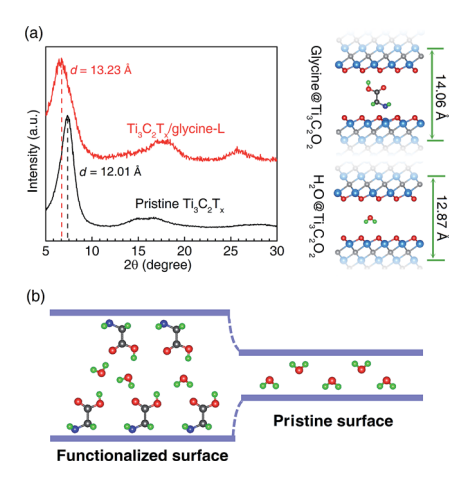


Fig. 3 (a) XRD patterns of the pristine  $d-Ti_3C_2T_x$ ,  $d-Ti_3C_2T_x$ /glycine films and predicted interlayer spacing for  $H_2O@Ti_3C_2O_2$  and glycine@ $Ti_3C_2O_2$ . (b) Schematic diagrams for pristine and glycine functionalized  $d-Ti_3C_2T_x$  surfaces.

Based on the above predictions, we plotted the optimized schematic diagram for glycine functionalized d- $\mathrm{Ti_3C_2T_x}$  surfaces (Fig. 3b). The hydrogen-bond network can be built between glycine and water molecules, which could facilitate diffusion of hydrogen ions. Meanwhile, compared with the pristine surface, the increased interlayer spacing contributed by the functionalized surface will lead to an improved ion accessibility, enhanced charging rate and better cycling performance.

To verify the effect of surface functionalization of d-Ti $_3$ C $_2$ T $_x$  by glycine on its charge storage, we conducted the cyclic voltammetry (CV) experiments for pristine d-Ti $_3$ C $_2$ T $_x$  (Fig. 4a) and d-Ti $_3$ C $_2$ T $_x$ /glycine (Fig. 4b) hybrids in 3 M H $_2$ SO $_4$  at various sweep rates ranging from 10 mV s $^{-1}$  to 1 V s $^{-1}$  in the potential window from -0.6 to 0.3 V *versus* Ag/AgCl. It is obvious from the CVs in Fig. 4b that at sweep rates below 20 mV s $^{-1}$  the peak separation is smaller than 0.1 V for d-Ti $_3$ C $_2$ T $_x$ /glycine hybrid, indicating fast surface redox reactions.

A comparison of the rate performances for pristine  $d-Ti_3C_2T_x$ and d-Ti<sub>3</sub>C<sub>2</sub>T<sub>x</sub>/glycine hybrid (Fig. 4c) shows that surface functionalization by glycine improved its performance especially at high scan rates, which could be ascribed to the combined effect of surface functionalization of the glycine and increased interlayer spacing. At a scan rate of 10 mV  $\rm s^{-1}$ , the capacitance of pristine d-Ti<sub>3</sub>C<sub>2</sub>T<sub>x</sub> increased from 299 F  $g^{-1}$  to 324 F  $g^{-1}$  for the d-Ti<sub>3</sub>C<sub>2</sub>T<sub>x</sub>/glycine hybrid. At a high rate of 1 V s<sup>-1</sup>, d-Ti<sub>3</sub>C<sub>2</sub>T<sub>x</sub>/ glycine hybrid electrodes could retain capacitance of 140 F g<sup>-1</sup>, which doubles the value of pristine  $d-Ti_3C_2T_x$  electrodes (Fig. 4c). At 1 V  $s^{-1}$ , the capacitance retention of pristine d-Ti<sub>3</sub>C<sub>2</sub>T<sub>x</sub> and d-Ti<sub>3</sub>C<sub>2</sub>T<sub>x</sub>/glycine was found to be 23.0% and 43.3%, respectively. When increasing the initial amount of glycine (d-Ti<sub>3</sub>C<sub>2</sub>T<sub>x</sub>/glycine-H), it still exhibits a good rate performance. However, increased loading of glycine might hinder ion transport. At the low scan rate, all the reactive sites can be occupied by electrolyte ions. The conductivity will be the dominant factor for capacitance. A higher content of nonconductive glycine leads to a lower conductivity, resulting in a lower capacitance of d-Ti<sub>3</sub>C<sub>2</sub>T<sub>x</sub>/glycine-H. At high scan rates,

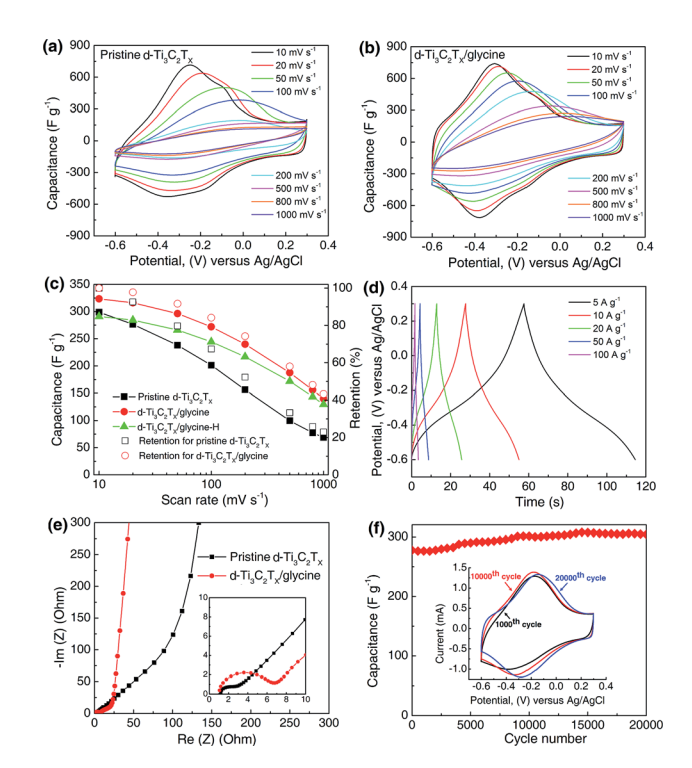


Fig. 4 (a and b) Cyclic voltammetry profiles at different scan rates for pristine  $d-Ti_3C_2T_x$  and  $d-Ti_3C_2T_x/glycine$  in 3 M  $H_2SO_4$ , (c) rate performance and capacitance retention for pristine  $d-Ti_3C_2T_x$ ,  $d-Ti_3C_2T_x/glycine$  and  $d-Ti_3C_2T_x/glycine$ -H (d) galvanostatic charge/discharge cycles of  $d-Ti_3C_2T_x/glycine$  at various current densities, (e) Nyquist plot of impedance, and (f) cycle life performance at the scan rate of  $100 \text{ mV s}^{-1}$  for  $d-Ti_3C_2T_x/glycine$ . Inset shows that the shape of the CVs was retained after long cycling.

there is not enough time for electrolyte ions to diffuse into the material deeply, resulting in the similar capacitances for both d- ${\rm Ti}_3{\rm C}_2{\rm T}_x$ /glycine and d- ${\rm Ti}_3{\rm C}_2{\rm T}_x$ /glycine-H. We also explored another amino acid, leucine, and showed that a better rate performance and retention could be obtained compared to pure MXene films (Fig. S5†).

The high coulombic efficiency near 100% shown in galvanostatic charge/discharge curves (Fig. 4d) at current densities of 5, 10, 20, 50 and 100 A g $^{-1}$  confirms the excellent reversibility of the redox reactions. Electrochemical impedance spectroscopy (Fig. 4e) displays smaller ion diffusion resistance for d $^{-}$ Ti $_3$ C $_2$ T $_x$ / glycine hybrid, due to increased interlayer spacing, as shown by the large slope of the plot at lower frequencies. Moreover, the electrodes showed good stability, with capacitance even slightly increasing after 20 000 cycles due to improved accessability of the interlayer spacing (Fig. 4f). Comparison of the initial and final CVs (inset in Fig. 4f) confirmed the stable electrochemical performance, which could be ascribed to the bonding between glycine and d $^{-}$ Ti $_3$ C $_2$ T $_x$ .

## Conclusions

In summary, using first principle calculations, we predicted the most stable configuration of glycine on  ${\rm Ti_3C_2O_2}$  with highest binding energy of -0.75 eV. The shared electrons between Ti

and N atoms suggest the formation of a Ti-N bond between glycine and Ti<sub>3</sub>C<sub>2</sub>O<sub>2</sub>. In addition, the flexible freestanding films of d-Ti<sub>3</sub>C<sub>2</sub>T<sub>x</sub>/glycine hybrids were prepared and XPS verified the presence of Ti-N bonding, supporting our theoretical predictions. The observed interlayer spacing of d-Ti<sub>3</sub>C<sub>2</sub>T<sub>r</sub>/glycine hybrid by XRD was 1.22 Å larger than that of pristine d-Ti<sub>3</sub>C<sub>2</sub>T<sub>r</sub>, in agreement with our prediction. Moreover, at a scan rate of 10 mV s<sup>-1</sup>, the capacitance reached 324 F g<sup>-1</sup> for d-Ti<sub>3</sub>C<sub>2</sub>T<sub>r</sub>/ glycine hybrid and more than 40% of this value was retained at 1 V s<sup>-1</sup>, twice the value of pristine MXene film. Besides, the electrodes showed good stability for more than 20 000 cycles. The enhanced rate and life cycling performances could be ascribed to the increased interlayer spacing and stable Ti-N bond.

# Conflicts of interest

Communication

There are no conflicts to declare.

# Acknowledgements

This work was supported by the Fluid Interface Reactions, Structures, and Transport (FIRST) Center, an Energy Frontier Research Center funded by the U.S. Department of Energy, Office of Science, Basic Energy Sciences. Chi Chen was supported by the Chinese Scholarship Council (CSC). The authors thank the Centralized Research Facilities of Drexel University for providing access to XRD, and TEM. The computational resources were provided by Intelligent Electronics Institute, Huazhong University of Science and Technology, China.

## Notes and references

- 1 P. Lazar, F. Karlicky, P. Jurecka, M. Kocman, E. Otyepkova, K. Safarova and M. Otyepka, J. Am. Chem. Soc., 2013, 135, 6372-6377.
- 2 S. Wickenburg, J. Lu, J. Lischner, H. Z. Tsai, A. A. Omrani, A. Riss, C. Karrasch, A. Bradley, H. S. Jung, R. Khajeh, D. Wong, K. Watanabe, T. Taniguchi, A. Zettl, A. H. Neto, S. G. Louie and M. F. Crommie, Nat. Commun., 2016, 7, 13553.
- 3 A. A. Tsukanov and S. G. Psakhie, Sci. Rep., 2016, 6, 19986.
- 4 A. Schlierf, P. Samorì and V. Palermo, J. Mater. Chem. C, 2014, 2, 3129.
- 5 J. M. Englert, C. Dotzer, G. Yang, M. Schmid, C. Papp, J. M. Gottfried, H. P. Steinruck, E. Spiecker, F. Hauke and A. Hirsch, Nat. Chem., 2011, 3, 279-286.
- 6 C. R. Ryder, J. D. Wood, S. A. Wells, Y. Yang, D. Jariwala, T. J. Marks, G. C. Schatz and M. C. Hersam, Nat. Chem., 2016, 8, 597-602.
- 7 Q. Li, Q. Zhou, X. Niu, Y. Zhao, Q. Chen and J. Wang, J. Phys. Chem. Lett., 2016, 7, 4540-4546.
- 8 Q. Tang and D.-e. Jiang, Chem. Mater., 2015, 27, 3743-3748.
- 9 S. Jiang, S. Butler, E. Bianco, O. D. Restrepo, W. Windl and J. E. Goldberger, Nat. Commun., 2014, 5, 3389.
- 10 B. D. Assresahegn, T. Brousse and D. Bélanger, Carbon, 2015, 92, 362-381.

- 11 M. Naguib, M. Kurtoglu, V. Presser, J. Lu, J. Niu, M. Heon, L. Hultman, Y. Gogotsi and M. W. Barsoum, Adv. Mater., 2011, 23, 4248-4253.
- 12 B. Anasori, Y. Xie, M. Beidaghi, J. Lu, B. C. Hosler, L. Hultman, P. R. C. Kent, Y. Gogotsi and M. W. Barsoum, ACS Nano, 2015, 9507-9516.
- 13 M. Naguib, V. N. Mochalin, M. W. Barsoum and Y. Gogotsi, Adv. Mater., 2014, 26, 992-1005.
- 14 J.-C. Lei, X. Zhang and Z. Zhou, Front. Phys., 2015, 10, 276-
- 15 X. Zhang, Z. Zhang and Z. Zhou, J. Energy Chem., 2018, 27,
- 16 M. Naguib and Y. Gogotsi, Acc. Chem. Res., 2015, 48, 128-135.
- 17 Q. Tang, Z. Zhou and P. Shen, J. Am. Chem. Soc., 2012, 134,
- 18 H. Li, Y. Hou, F. Wang, M. R. Lohe, X. Zhuang, L. Niu and X. Feng, Adv. Energy Mater., 2016, 7, 1601847.
- 19 B. Aïssa, A. Ali, K. A. Mahmoud, T. Haddad and M. Nedil, Appl. Phys. Lett., 2016, 109, 043109.
- 20 M. Q. Zhao, C. E. Ren, Z. Ling, M. R. Lukatskaya, C. Zhang, K. L. Van Aken, M. W. Barsoum and Y. Gogotsi, Adv. Mater., 2015, 27, 339-345.
- 21 Y. Dall'Agnese, P. Rozier, P.-L. Taberna, Y. Gogotsi and P. Simon, J. Power Sources, 2016, 306, 510-515.
- 22 M.-Q. Zhao, M. Torelli, C. E. Ren, M. Ghidiu, Z. Ling, B. Anasori, M. W. Barsoum and Y. Gogotsi, Nano Energy, 2016, 30, 603-613.
- 23 Q. Xue, Z. Pei, Y. Huang, M. Zhu, Z. Tang, H. Li, Y. Huang, N. Li, H. Zhang and C. Zhi, J. Mater. Chem. A, 2017, 5, 20818-20823.
- 24 F. Shahzad, M. Alhabeb, C. B. Hatter, B. Anasori, S. M. Hong, C. M. Koo and Y. Gogotsi, Science, 2016, 353, 1137-1140.
- 25 M. Alhabeb, K. Maleski, B. Anasori, P. Lelyukh, L. Clark, S. Sin and Y. Gogotsi, Chem. Mater., 2017, 29, 7633-7644.
- 26 Z. Ling, C. E. Ren, M.-Q. Zhao, J. Yang, J. M. Giammarco, J. Qiu, M. W. Barsoum and Y. Gogotsi, Proc. Natl. Acad. Sci. U. S. A., 2014, 111, 16676-16681.
- 27 C. Chen, M. Boota, X. Xie, M.-Q. Zhao, B. Anasori, C. E. Ren, L. Miao, J. Jiang and Y. Gogotsi, J. Mater. Chem. A, 2017, 5, 5260-5265.
- 28 M. Zhu, Y. Huang, Q. Deng, J. Zhou, Z. Pei, Q. Xue, Y. Huang, Z. Wang, H. Li, Q. Huang and C. Zhi, Adv. Energy Mater., 2016, 6, 1600969.
- 29 O. Mashtalir, M. Naguib, V. N. Mochalin, Y. Dall'Agnese, M. Heon, M. W. Barsoum and Y. Gogotsi, Nat. Commun., 2013, 4, 1716.
- 30 J. Xuan, Z. Wang, Y. Chen, D. Liang, L. Cheng, X. Yang, Z. Liu, R. Ma, T. Sasaki and F. Geng, Angew. Chem., Int. Ed., 2016, 55, 1-7.
- 31 O. Mashtalir, M. R. Lukatskaya, M. Q. Zhao, M. W. Barsoum and Y. Gogotsi, Adv. Mater., 2015, 27, 3501-3506.
- 32 P. Singla, M. Riyaz, S. Singhal and N. Goel, Phys. Chem. Chem. Phys., 2016, 18, 5597-5604.
- 33 H. T. Larijani, M. Jahanshahi, M. D. Ganji and M. H. Kiani, Phys. Chem. Chem. Phys., 2017, 19, 1896-1908.
- 34 S. Pandit and M. De, J. Phys. Chem. C, 2017, 121, 600-608.

- 35 C. K. Chua and M. Pumera, *Chem. Soc. Rev.*, 2014, 43, 291–312.
- 36 E. Satheeshkumar, A. Bandyopadhyay, M. B. Sreedhara, S. K. Pati, C. N. R. Rao and M. Yoshimura, *ChemNanoMat*, 2017, 3, 172–177.
- 37 J. Xuan, Z. Wang, Y. Chen, D. Liang, L. Cheng, X. Yang, Z. Liu, R. Ma, T. Sasaki and F. Geng, *Angew. Chem., Int. Ed.*, 2016, 128, 14789–14794.
- 38 K. Rasool, M. Helal, A. Ali, C. E. Ren, Y. Gogotsi and K. A. Mahmoud, *ACS Nano*, 2016, **10**, 3674–3684.
- 39 Q. Xue, H. Zhang, M. Zhu, Z. Pei, H. Li, Z. Wang, Y. Huang, Y. Huang, Q. Deng, J. Zhou, S. Du, Q. Huang and C. Zhi, *Adv. Mater.*, 2017, 29, 1604847.
- 40 G. Kresse and J. Furthmüller, *Phys. Rev. B: Condens. Matter Mater. Phys.*, 1996, **54**, 11169.
- 41 P. Homenberg and W. Kohn, *Phys. Rev.*, 1964, **136**, B864-B871.
- 42 W. Kohn and L. J. Sham, Phys. Rev., 1965, 140, A1133-A1138.
- 43 J. P. Perdew, K. Burke and M. Ernzerhof, *Phys. Rev. Lett.*, 1996, 77, 3865.
- 44 J. Klimeš, D. R. Bowler and A. Michaelides, *J. Phys.: Condens. Matter*, 2010, **22**, 022201.
- 45 J. Klimeš, D. R. Bowler and A. Michaelides, *Phys. Rev. B: Condens. Matter Mater. Phys.*, 2011, **83**, 195131.
- 46 M. A. Hope, A. C. Forse, K. J. Griffith, M. R. Lukatskaya, M. Ghidiu, Y. Gogotsi and C. P. Grey, *Phys. Chem. Chem. Phys.*, 2016, **18**, 5099–5102.
- 47 H. J. Monkhorst and J. D. Pack, *Phys. Rev. B: Solid State*, 1976, 13, 5188–5192.
- 48 K. Momma and F. Izumi, J. Appl. Crystallogr., 2008, 41, 653.
- 49 R. F. W. Bader, Atoms in Molecules: A Quantum Theory, Oxford University Press, Oxford, UK, 1990.

- 50 R. S. Krishnan and K. Balasubramanian, *Proc.-Indian Acad. Sci., Sect. A*, 1958, **48**, 55–61.
- 51 X. Yang, J. Lu, X. Wang and C. B. Ching, *J. Raman Spectrosc.*, 2008, **39**, 1433–1439.
- 52 J. Baran and H. Ratajczak, Vib. Spectrosc., 2007, 43, 125-139.
- 53 K. Balasubramanian, R. S. Krishnan and Y. Iitaka, *Bull. Chem. Soc. Jpn.*, 1962, 35, 1303–1305.
- 54 K. Furić, V. Mohaček, M. Bonifačić and I. Štefanić, *J. Mol. Struct.*, 1992, **267**, 39–44.
- 55 A. Gómez-Zavaglia and R. Fausto, *Phys. Chem. Chem. Phys.*, 2003, 5, 3154–3161.
- 56 M. T. Rosadoa, M. L. T. S. Duartea and R. Fausto, *Vib. Spectrosc.*, 1998, **16**, 35–54.
- 57 S. Sankar, M. R. Manikandan, S. D. Gopal Ram, T. Mahalingam and G. Ravi, *J. Cryst. Growth*, 2010, **312**, 2729–2733.
- 58 A. Y. Ivanov, G. Sheina and Y. P. Blagoi, Spectrochim. Acta, Part A, 1998, 55, 219–228.
- 59 N. C. Saha and H. G. Tompkins, *J. Appl. Phys.*, 1992, 72, 3072–3079.
- 60 B. M. Biwer and S. L. Bernasek, Surf. Sci., 1986, 167, 207-230.
- 61 U. Diebold and T. E. Madey, J. Vac. Sci. Technol., A, 1992, 10, 2327–2335.
- 62 S. Kajiyama, L. Szabova, K. Sodeyama, H. Iinuma, R. Morita, K. Gotoh, Y. Tateyama, M. Okubo and A. Yamada, ACS Nano, 2016, 10, 3334–3341.
- 63 T. Hu, M. Hu, Z. Li, H. Zhang, C. Zhang, J. Wang and X. Wang, *Phys. Chem. Chem. Phys.*, 2016, 18, 20256–20260.
- 64 M. Ghidiu, M. R. Lukatskaya, M. Q. Zhao, Y. Gogotsi and M. W. Barsoum, *Nature*, 2014, **516**, 78–81.
- 65 V. Augustyn, J. Come, M. A. Lowe, J. W. Kim, P. L. Taberna, S. H. Tolbert, H. D. Abruna, P. Simon and B. Dunn, *Nat. Mater.*, 2013, 12, 518–522.